Structural Eng./Earthquake Eng., JSCE, Vol. 15, No. 1, 63s—72s, 1998 April
(J. Struct. Mech. Earthquake Eng., JSCE, No. 591/ I —43)

SIMULATION FOR ANALYSING DIRECT DERAILMENT LIMIT OF RUNNING VEHICLE ON OSCILLATING TRACKS

Akio MATSUURA

Member of J.S.C.E, Dr.of Eng, Professor, Dpt.of Civil Eng. Kanazawa Institute of Technology
(7-1 Ogigaoka Nonoichi Ishikawa 921, Japan)

A practical simulation method for analysing direct derailment limit of running vehicle for high speed train on oscillating track under an earthquake using a 3 dimensional one vehicle model was proposed. In this method, the Kalker's simple theory and a newly introduced 2 point contact algorithm were applied to estimation of wheel/rail contact force. These application carried a possibility of *direct* derailment estimation which differed from previous *indirect* derailment estimation. It was clarified that the jumping derailment occurred at lower lateral frequency of track oscillation but the mounting derailment did at higher frequency and that the derailment limit of track amplitude showed larger value than that of indirect previous method.

Key Words *: running safety, oscillating track, railway vehicle, mechanical model, dynamic interaction*

1. PREFACE

Authors have reported a paper on running safety of railway vehicle on oscillating track using a mechanical model with vertical wheel flanges [1]. In that paper, past studies on the running safety of railway vehicle on oscillating tracks [2), 3), 4)] were briefly reviewed. And so called the Levi-Chartet formula was simply used there to estimate the wheel/rail contact forces. Finally, it proposed a tentative limitation of ground acceleration for estimating the running safety of railway vehicles taking into account 'a wheel separation height from the rail' as well as 'the ratio of lateral load to wheel load (Q/P)'.

However, the safety estimation only with the wheel separation height or with Q/P is not sufficient to find the derailment itself. That is, the derailment was estimated *indirectly* in the former studies. Therefore, it will be necessary to improve the way of computer simulation, especially in the analysis of the wheel/rail contact mechanism, and necessary to simulate *directly* the time process of derailment and obtain its limit for more reasonable safety estimation of the railway vehicle on the oscillating track.

For this purpose, the Kalker's nonlinear creep theory [5], the most accurate method at present, for estimating the wheel/rail contact forces will be used in this paper. By using this theory, a direct simulation method which is able to pursue the movement up to the real derailment of running vehicle on oscillating tracks will be proposed. As numerical examples, simulation results on the dynamic response of railway vehicle shaken by an earthquake and a tentative safety limit for laterally oscillating tracks will be shown.

2. OUTLINE OF DYNAMIC MODEL

Main analytical assumptions for dynamic model are shown as follows. Here assumptions 8), 9), 10) correspond to those in the reference 1).

1) Sectional profiles of wheel tread or flange and rail top are defined arbitrary.
2) Wheel/rail contact forces are obtained by the Kalker's nonlinear creep theory.
3) Wheel/rail contact geometrical properties in sectional profile are defined by a wheel/rail relative displacement and are never affected directly by the yaw motion of wheelset [6], except for longitudinal property.
4) Status whether the wheel is in contact with the

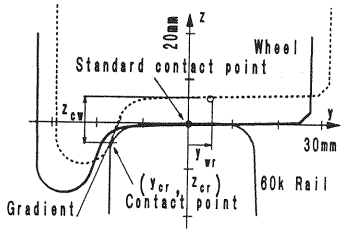

Fig.1 Sectional profiles and standard contact state

rail at one point or two points or it does not contact at all is to be discriminated by the wheel/rail relative displacement.

5) The rail is to be replaced with a dynamic system having equivalent mass, damping and spring which are moving longitudinally together with the wheel.
6) The equivalent mass of rail is only considered for the lateral movement.
7) Both of the vertical and lateral equivalent spring constants of rail [7] are calculated by the practical solution for the torsion of rail proposed by Hoshino [8], adding their nonlinear property.
8) The railway vehicle is the ordinary 2 axle bogy car for high speed train composed of 1 car body, 2 trucks and 4 wheelsets.
9) The car body is connected with the trucks by nonlinear secondary springs and bolster anchors, and the trucks are connected with the wheelsets by nonlinear axle springs.
10) A non-linearity caused by a component shift of vertical and lateral spring forces with the roll motion of vehicle is taken into account.
11) The wheelsets, trucks and car body are assumed to be rigid bodies except at the narrow contact portion of wheelsets in calculating the wheel/rail contact forces.
12) The rail deflection as an beam action in bending and torsion is considered. On the other hand, the elastic deformation of rail section is neglected. But a small elastic deformation of rail at the narrow wheel/rail contact portion is considered.
13) Any kind of the gyro effect is neglected, because it will be considered to be comparatively small.

The 3 dimensional coordinate axes x, y, z denote longitudinal, lateral and vertical, respectively.

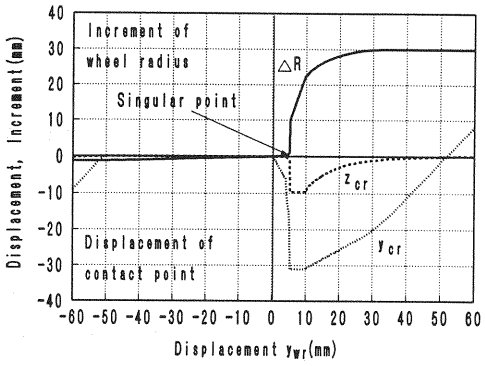

Fig.2 Contact point and wheel radius increment

3. FUNDAMENTAL PROPERTIES OF WHEEL AND RAIL

(1) Wheel/rail contact geometrical properties

A coordinate origin of wheel or that of rail is defined to be the contact point of wheel and rail in their standard contact position. The wheel/rail contact geometrical properties should be calculated in advance in relation to the wheel/rail relative displacement,

$$y_{wr} = y_w \pm r\,\overline{\phi}_w - y_r \qquad (1)$$

where, $y_w$is the lateral displacement of the wheel -set, $\overline{\phi}_w$ an equivalent non-linear roll angle of wheelset defined by an expression with the real roll angle ϕ_w as $\overline{\phi}_w = \sin\phi_w + b/r(\cos\phi_w - 1)$, y_r the lateral displacement of the rail, b a half distance between the standard contact points of right and left wheels, and r the standard wheel radius. The sign $\pm$ is applied to the right/left side of the wheel or rail, respectively.

For example, some contact geometrical properties for the standard wheel section of Shinkansen [9] and that of the 60 kg/m rail are shown above. Sectional profiles for the standard contact state are illustrated in **Fig.1**. A wheel radius increment ΔR, contact coordinates y_{cr} and z_{cr} for y_{wr} are shown in **Fig.2**.

The actual radius of wheel is $R = r + \Delta R$. The contact coordinate on the wheel z_{cw} indicated in **Fig.1** will be calculated easily. A wheel tread gradient γ and a ratio of semi-axis of contact ellipsoid a_e/b_e for y_{wr} are shown in **Fig.3**.

The longitudinal and lateral semi-axes a_e, b_e

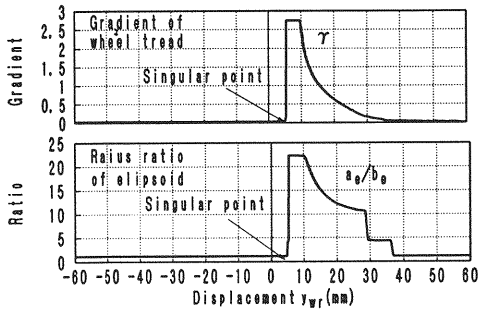

Fig.3 Tread gradient and contact ellipsoid

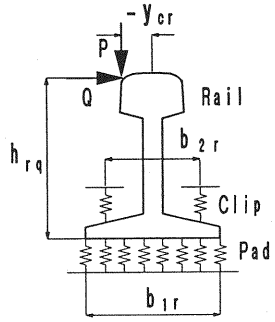

Fig.4 Mechanical model for estimating equivalent spring constants of rail

of the ellipsoid occurring at the wheel/rail contact point are calculated with a normal component of the contact normal force, an effective radius of wheel, the sectional radius of the wheel and that of the rail at the contact point [10] where the effective radius of wheel is expressed by $r/\cos\gamma$ that will be described on a declined y-plane by angle equal to γ around x-axis containing the contact point.

On the other hand, a contact point on the wheel for longitudinal coordinate is expressed by

$$x_{cw} = \gamma r(\psi_w - \psi_r) \tag{2}$$

where, ψ_w is the yaw angle of the wheelset and ψ_r the alignment angle of the rail that will be given by Eq.(35).

(2) Wheel/rail contact force in nonlinear creep theory

The longitudinal creepage c_{rx} and the lateral one c_{ry} and the spin c_{rxy} on the wheel/rail contact surface are

$$c_{rx} = -\{b\dot{\psi}_w + (R-r)\frac{v}{r}\}\frac{1}{v} \tag{3a}$$

$$c_{ry} = \{\dot{y}_w + r\dot{\phi}_w - v\psi_w - (\dot{y}_r - \dot{y}_{gs})\}\frac{1}{v\cos\gamma} \tag{3b}$$

$$c_{rxy} = -\{\frac{v}{R}(\sin\gamma - \dot{\phi}_w\cos\gamma) - \psi_w\cos\gamma\}\frac{1}{v} \tag{3c}$$

respectively, where, v is the rolling velocity of wheel or running velocity of vehicle, y_{gs} a static lateral displacement of track estimated from the track irregularity that will be shown in section **5.**, and (•) means the first differentiation in time.

The creep forces will be derived using the Kalker's nonlinear creep theory. *Linear* forces ΔS_x and ΔS_y for x and y directions respectively, at the point (x, y) in a small area ΔA are calculated by

$$\Delta S_x = (\frac{c_{rx}}{L_1} - \frac{c_{rxy}}{L_3})(x - x_0)\Delta A \tag{4a}$$

$$\Delta S_y = \{\frac{c_{ry}(x-x_0)}{L_2} + \frac{c_{rxy}(x^2 - x_0^2)}{L_3}\}\Delta A \tag{4b}$$

where, $x_0^2 = 1 - y^2/b_e^2$, and

$$L_1 = \frac{8a_e}{3C_{11}G},\ L_2 = \frac{8a_e}{3C_{22}G},\ L_3 = \frac{a_e\pi}{4C_{23}G}\sqrt{\frac{a_e}{b_e}} \tag{5}$$

in which G is the modulus of rigidity of steel, C_{11}, C_{22}, C_{23} are the Kalker's coefficients defined with a_e and b_e [11].

Then, the *nonlinear* creep forces ΔT_x and ΔT_y in the small area are estimated according to the mechanical condition whether the contact state is in adhesion or slip using the total linear force

$$\Delta S = \sqrt{\Delta S_x^2 + \Delta S_y^2} \tag{6}$$

and the maximum friction force

$$\Delta F = \frac{2\mu N\{a_e^2 b_e^2 - b_e^2 x^2 - a_e^2 y^2\}}{a_e^3 b_e^3 \pi}\Delta A \tag{7}$$

where, μ is the coefficient of friction.

Finally, nonlinear creep forces in the contact ellipsoid area are obtained as

$$T_x = \sum\Delta T_x,\quad T_y = \sum\Delta T_y \tag{8}$$

The normal force N is estimated by

$$N = P\cos\gamma + Q\sin\gamma \tag{9}$$

where P is a wheel load which will be given in Eq.(17) with a few state quantities. On the other hand, the lateral load Q will be estimated by

$$Q = P\tan\gamma - T_y. \tag{10}$$

(3) Equivalent spring constants of rail

Referring the mechanical model [7] shown in **Fig.4**, equivalent spring constants for lateral k_{ry} and for vertical k_{rz} will be expressed by

$$k_{ry}=\frac{1}{dh_0^2+\frac{\beta_y}{2K_y}},\qquad k_{rz}=\frac{k_{rz}'}{1+y_{cr}^2 h_{rq}\frac{k_{rz}'}{k_{ry}}} \tag{11}$$

where d is an inverse of equivalent torsional spring constant around the shear center of rail induced by Hoshino [8] that will be expressed by

$$d=\frac{a_r k_f n(a_r\alpha-1)(1+\frac{a_r\beta_y h_{2r}}{2h_0})+(1+\frac{h_{2r}}{h_0})\alpha C}{a_r k_f\{a_r k_f\alpha n(a_r\alpha-1)+(1+2n)\alpha C\}} \tag{12}$$

in which $\alpha=(C/C_w)^{1/2}$ and $\beta_y=\{K_y/(4EI_y)\}^{1/4}$.

In Eq.(11) and (12), h_0 is a distance of the loading point from the shear centre, K_y a lateral spring constant of the fastening device per unit length, h_{rq} a distance of a loading point of the lateral load from the rail base, a_r a rail fastening distance, n (=1.7) a weight parameter for reaction of several fastening devices for approximation, C the torsional rigidity, C_w the bending torsional rigidity of rail, h_{2r} a distance of the shear centre from the rail base, EI_y the bending rigidity of rail in horizontal plane.

Also, k_{rz}' is an equivalent spring constant for the normal axis of rail as shown

$$k_{rz}'=8EI_z\beta_z^3/\{e^{-\zeta_z}(\cos\zeta_z+\sin\zeta_z)\} \tag{13}$$

where, $\beta_z=\{D/(4EI_z)\}^{1/4}$, $\zeta_z=a_r\beta_z/2$, D is the ballast sinking coefficient per unit length, EI_z the bending rigidity of rail in vertical plane.

Further, k_f is an anti-tilt coefficient of the rail fastening device which, in case of the tilt-angle satisfies $\theta<\theta_1$, is calculated by

$$k_f=\frac{1}{a_r}(\frac{k_{1r}b_{1r}^2}{12}+\frac{k_{2r}b_{2r}^2}{2}) \tag{14}$$

or, in case of $\theta\geq\theta_1$, that is the condition of partial separation of rail base and rail pad, by

$$k_f=\{\frac{k_{1r}x^2}{2b_{1r}}(\frac{b_{1r}}{2}-\frac{x}{3})+\frac{k_{2r}b_{2r}}{2}(\frac{b_{1r}+b_{2r}}{2}-x)\}\frac{1}{a_r} \tag{15}$$

where, b_{1r} is the width of the rail pad, b_{2r} the distance between the fastening clips, k_{1r} the spring constant of rail pad, k_{2r} the spring constant of clip. On the other hand, the parameter x and θ_1 with the rail pressure w_1 are defined by

$$x=-k_{2r}+\frac{b_{1r}}{k_{1r}}\sqrt{k_{2r}^2+\frac{b_{1r}+b_{2r}}{b_{1r}}k_{1r}k_{2r}+\frac{2k_{1r}w_1}{b_{1r}\theta_1}} \tag{16a}$$

$$\theta_1=\frac{2w_1}{b_{1r}k_{1r}},\qquad w_1=P\{1-e^{-\zeta_z}\cos\zeta_z\}. \tag{16b}$$

The equivalent damping factors of the rail for lateral and vertical directions are denoted as c_{ry} and c_{rz}, respectively. An additional lateral displacement of the rail y_p affected by the wheel load and its corresponding contact points will be expressed in a simple formula, easily.

4. DYNAMIC MODEL OF VEHICLE AND TRACK

(1) Wheel load and lateral load

Using Eq.(11), the wheel load P is written by

$$P=-k_{rz}(z_r-z_g)-c_{rz}(\dot{z}_r-\dot{z}_g)+P_s\geq 0 \tag{17}$$

where, z_g, which will be given by Eq.(34), is a forced vertical displacement of the track at the wheel position, and $P_s=(m_b+m_t+2m_w)g/4$ is the static wheel load, with the gravitational acceleration g, a vehicle body mass m_b, a vehicle truck mass m_t and a wheelset mass m_w, and z_r is the vertical displacement of rail that will be expressed by the status values and the wheel/rail contact geometrical properties with a vertical displacement of wheelset z_w as

$$z_r=z_w\pm b\,\overline{\phi}_w+r+z_{cw}+z_{cr}. \tag{18}$$

A lateral load acting on an anti-derailment guard installed inside the track will be expressed by

$$Q_G=k_{Gy}(-y_w+y_g-u_G)+c_{Gy}(-\dot{y}_w+\dot{y}_g)\geq 0 \tag{19}$$

where, k_{Gy} is the lateral spring constant of anti-derailment guard, c_{Gy} the damping coefficient of it, y_g a forced lateral displacement of the track that will be given by Eq.(34) and u_G a wheel flange back face clearance to the anti-derailment guard [12]. Here, the mass of the anti-derailment guard is neglected.

Subtracting the lateral load acting on the anti-derailment guard given by Eq.(19) from the lateral load acting on the rail given by Eq.(10), the lateral load acting on the wheel is obtained as

$$Q_w=Q-Q_G. \tag{20}$$

Increasing the relative displacement y_{wr}, we can find a singular point in the wheel/rail contact geometric properties as shown in **Fig.2** or **3**. This is a shifting point which moves from 'the wheel *tread* contact state' to 'the wheel *flange* contact state'. According to the sectional profile of wheel and rail, the shifting point appears smoothly or abruptly. If it appears smoothly, no problems will be found on the process of numerical analysis. But when it appears abruptly, the problems like numerical divergence are to be presumed.

To avoid these problems, here a concept of two

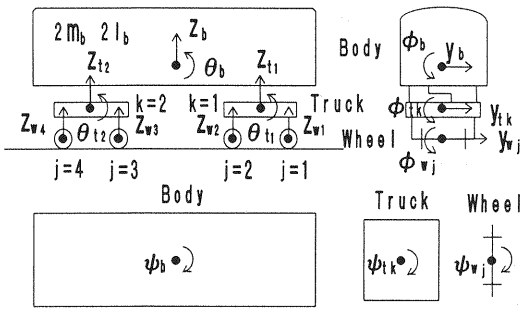

Fig.5 One vehicle model

point contact condition is newly introduced in algorithm. It will be shown as follows.

If the wheel/rail relative displacement satisfies

$$y_T < y_{wr} < y_F, \tag{21}$$

the contact status is regarded as in a 2 point condition where y_T is the maximum of the wheel/rail relative displacement which is in the wheel tread contact status, and y_F the minimum of that which is in the wheel flange contact status.

The wheel load will be divided into two parts, that is P_T acting on the wheel tread and P_F acting on the wheel flange, simultaneously. One of the most simple expressions for that will be

$$P_F = \frac{y_{wr} - y_T}{y_F - y_T} P, \quad P_T = P - P_F. \tag{22}$$

The lateral force Q_T for wheel tread and Q_F for wheel flange are computed by Eq.(10) using Eq.(22), and each wheel/rail contact geometrical property. At the same time the lateral load is expressed by

$$Q = Q_T + Q_F. \tag{23}$$

In practice, the length of 2 point contact section have to be defined sufficiently small not to affect the dynamic property of the whole model. The most simple expression may be proposed for the small length as

$$y_e = y_F - y_T \tag{24}$$

where

$$y_e = \frac{(a_e \sqrt[3]{P\cos\gamma_F + Q\sin\gamma_F})^2}{2r_F \sin\gamma_F} \tag{25}$$

which is the component of y in wheel's local deformation induced by an elastic contact forces, assuming that both of the wheel load and the lateral load act only on the wheel flange where γ_F is the gradient and r_F is the radius of rail section at the contact point of the wheel flange.

(2) Coordinates and symbols

Vehicle masses, momentum inertias and their coordinates are shown in **Fig.5**. In the next, parameters for ith wheel, for jth wheelset or for kth truck should be detected by suffixes i=1 ~ 8, j=1 ~ 4 and k=1 ~ 2 added to each parameter at the last position, respectively.

The wheelset and truck numbers will be counted starting from the front wheelset. The numbers of the right side wheel and the left side wheel in the jth wheelset will be i=2j−1, i=2j, respectively. And numbers of bolster anchor of right side and that of left side in the kth truck will be j=2k−1, j=2k, respectively.

A status vector of vehicle is defined as

$$\begin{aligned} \boldsymbol{y}_v = (&\dot{y}_w, \dot{z}_w, \dot{\phi}_w, \dot{\psi}_w, \dot{y}_t, \dot{z}_t, \dot{\phi}_t, \dot{\theta}_t, \dot{\psi}_t, \\ &\dot{y}_b, \dot{z}_b, \dot{\phi}_b, \dot{\theta}_b, \dot{\psi}_b, y_w, z_w, \phi_w, \psi_w, \\ &y_t, z_t, \phi_t, \theta_t, \psi_t, y_b, z_b, \phi_b, \theta_b, \psi_b)^T \end{aligned} \tag{26}$$

where each element of this vector is expressed by sub-vector, for example

$$\boldsymbol{y}_w = (y_{w,1}, y_{w,2}, y_{w,3}, y_{w,4})^T. \tag{27}$$

Corresponding with the status vector a mass matrix of vehicle is defined as

$$\begin{aligned} \boldsymbol{m}_v = \mathrm{Diag.}(&m_w, m_w, I_w, I_w, m_t, m_t, I_{tx}, \\ &I_{ty}, I_{tz}, 2m_b, 2m_b, 2I_{bx}, 2I_{by}, 2I_{bz}) \end{aligned} \tag{28}$$

where, suffix T means the transpose and Diag.(*) the diagonal matrix of which elements are *s, respectively. Each element of this matrix is expressed by sub-matrix, for example

$$\boldsymbol{m}_w = \mathrm{Diag.}(m_w, m_w, m_w). \tag{29}$$

A wheel load vector $\boldsymbol{P}$ and a lateral force vector $\boldsymbol{Q}_w$ are obtained by Eq.(17) and Eq.(20), which will be able to express by the status vectors.

The torque $T_{w,j}$ around the z axis acting on the jth wheelset caused by the longitudinal creep forces given by Eq.(8), the lateral forces given by Eq.(20) and the longitudinal contact points given by Eq.(2) on the right side ($i_1 = 2j-1$) and left side ($i_2 = 2j$) is written

$$T_{w,j} = (T_{x,i_1} + T_{x,i_2})b + (Q_{w,i_1} x_{cw,i_1} + Q_{w,i_2} x_{cw,i_2}). \tag{30}$$

A torque vector $\boldsymbol{T}_w$ will be obtained using these expressions.

A status vector of rail is defined as

$$\boldsymbol{y}_r = (\dot{y}_{r,1}, \dot{y}_{r,2} \cdots \dot{y}_{r,8}, y_{r,1}, y_{r,2} \cdots y_{r,8})^T \tag{31}$$

where $y_{r,i}$ denotes the lateral displacement of the ith rail toward the outer direction of the track. Corresponding with this vector a mass matrix of

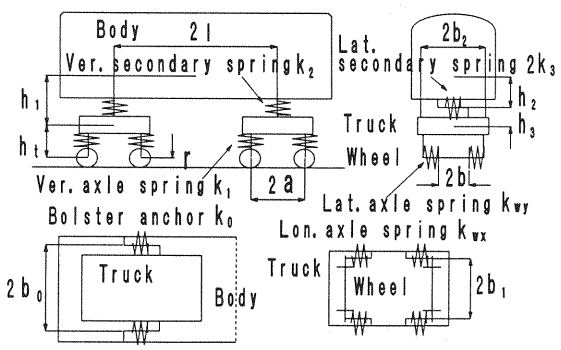

Fig.6 Dimensions/symbols of one vehicle model

rail is defined as

$$\boldsymbol{m}_r = \mathrm{Diag.}(m_r, m_r, m_r, m_r, m_r, m_r). \quad (32)$$

A lateral force vector $\boldsymbol{Q}$ will be obtained with Eq.(23).

(3) Vehicle spring forces

Spring contraction vector of vehicle $\boldsymbol{q}_v$ is obtained with the vehicle dimensions and the status vector by the ordinary method. The corresponding spring force vector will be obtained as a function of the spring contraction vector of vehicle as shown

$$\boldsymbol{R}_v = \boldsymbol{K}\{\boldsymbol{q}_v(\boldsymbol{y}_v)\} \quad (33)$$

where $\boldsymbol{K}$ is a vector function which connects the spring contractions and spring forces with bilinear property caused by the spring stoppers. And in that function, the acting points of vertical and lateral vehicle springs are modified for the sake of non-linearity relating to the lateral displacement and the roll angles of the body and trucks.

The vehicle parameters used in the above equations are shown in **Fig.6**.

5. DYNAMIC EQUATIONS

The track is assumed to oscillate laterally and vertically having track irregularities in lateral and vertical directions. The time functions of lateral oscillation and vertical one are $y_{gd}(t)$ and $z_{gd}(t)$, and the space functions of lateral irregularity and horizontal one are $y_{gs}(x)$ and $z_{gs}(x)$, respectively.

Using a longitudinal displacement of jth wheelset $x_j(t)$, for example $x_1(t) = vt$ for 1st wheelset, the lateral and vertical displacements of track under the ith wheel at the arbitrary time are, respectively.

$$y_{g,i} = y_{gd}(t) + y_{gs}\{x_j(t)\} \quad (34a)$$

$$z_{g,i} = z_{gd}(t) + z_{gs}\{x_j(t)\}. \quad (34b)$$

Using the lateral irregularity of track, the alignment angle of rail under the ith wheel is

$$\psi_{r,i} = \frac{\dot{y}_{gs}\{x_j(t)\}}{v}. \quad (35)$$

The dynamic equation of ith rail for lateral direction is obtained as

$$m_r \ddot{y}_{r,i} = k_{ry,i}(y_{r,i} - y_{P,i} - y_{g,i}) - c_{ry,i}(\dot{y}_{r,i} - \dot{y}_{g,i}) - Q_i \quad (36)$$

where $y_{P,i}$ is expressed by the wheel load as mentioned in **3(3)**. Defining a new vector, that is a forced displacement vector of track as

$$\boldsymbol{y}_g = (\dot{y}_{g,1} \cdots \dot{y}_{g,4}, y_{g,1} \cdots y_{g,4})^T \quad (37)$$

the dynamic equations for the lateral movement of the rail is obtained in matrix form as

$$\begin{pmatrix} m_r & 0 \\ 0 & I \end{pmatrix} \dot{\boldsymbol{y}}_r = \boldsymbol{C}(\boldsymbol{P}, \boldsymbol{Q}, \boldsymbol{y}_r) + \boldsymbol{D}(\boldsymbol{y}_g) \quad (38)$$

where $\boldsymbol{C}$ is a vector function of the contact forces $\boldsymbol{P}$, $\boldsymbol{Q}$ expressed by the status vectors $\boldsymbol{y}_v$, $\boldsymbol{y}_r$, and also $\boldsymbol{D}$ is a forced vector function of outer forces induced by the forced displacement of track $\boldsymbol{y}_g$.

The dynamic equation for the vehicle is given by

$$\begin{pmatrix} m_v & 0 \\ 0 & I \end{pmatrix} \dot{\boldsymbol{y}}_v = \boldsymbol{B}(\boldsymbol{P}, \boldsymbol{Q}_w, \boldsymbol{T}_w, \boldsymbol{R}_v, \boldsymbol{y}_v) \quad (39)$$

where, $\boldsymbol{B}$ is a vector function of the inner spring forces $\boldsymbol{R}_v$ given by Eq.(33), the wheel/rail contact forces $\boldsymbol{P}$, $\boldsymbol{Q}_w$ and $\boldsymbol{T}_w$. These are expressed by the status vectors $\boldsymbol{y}_v$, $\boldsymbol{y}_r$, and the forced displacement of track $\boldsymbol{y}_g$.

The dynamic equations of rail and vehicle are connected by the lateral loads $\boldsymbol{Q}$, $\boldsymbol{Q}_w$ and $\boldsymbol{Q}_G$ as given by Eq.(20).

6. SIMULATION EXAMPLES

In this section, a few numerical examples will be shown. The standard parameters of Shinkansen vehicle used here are the same as those used in the former paper [1]. The main parameters for the rail and track used here are as follows;

$m_r = 0.1\mathrm{t}$, $h_{rq} = 0.174\mathrm{m}$, $b_{1r} = 0.138\mathrm{m}$, $b_{2r} = 0.103\mathrm{m}$,

$h_0 = 0.136\mathrm{m}$, $k_{1r} = 89{,}000\mathrm{kN/m}$, $k_{2r} = 5{,}780\mathrm{kN/m}$,

$a_r = 0.6\mathrm{m}$, $C = 230.3\mathrm{kNm}^2$, $C_w = 3.26\mathrm{kNm}^4$, $D = \infty\mathrm{kN/m}^2$

$K_y = 19{,}600\mathrm{kN/m}$, $EI_y = 1{,}072\mathrm{kNm}^2$, $EI_z = 6{,}359\mathrm{kNm}^2$.

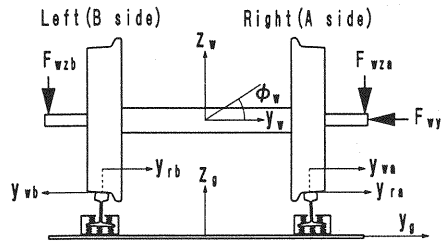

Fig.7 One wheel set model

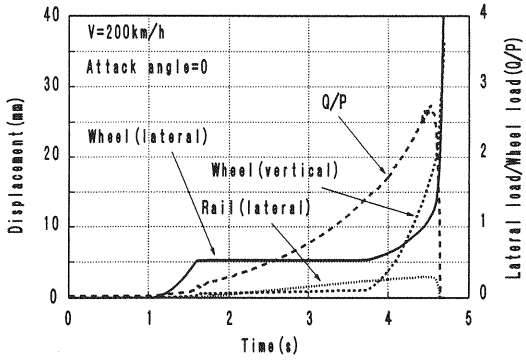

Fig.8 Response curve of Q/P

As for the numerical integration, the two contact conditions of Eq.(22) and (25) are used, and the Runge-Kutta-Gill method was used with step time interval of 1/1000 sec. for the wheel tread contact, 1/5000 sec. for the wheel flange contact state. These step intervals are determined to be nearly equal to 1/30 times of the lowest natural period of rail lateral vibration. The lateral natural frequency of the rail moving together with the wheelset in the wheel tread contact state is estimated as about 30 Hz, on the other hand in the wheel flange contact state it is estimated as about 100-150 Hz which is the lateral natural frequency of rail top.

In the following examples, the right-side and left-side wheels are also written as A-side and B-side, respectively. And suffixes a and b are used for the corresponding forces.

(1) Simulation on mounting derailment

Simulation results on mounting derailment will be shown here for a single wheelset. The wheelset is assumed to be subjected to forces

$$F_{wza}=P_s-\alpha F_v,\ F_{wzb}=P_s+\alpha F_v,\ F_{wy}=\alpha F_h$$

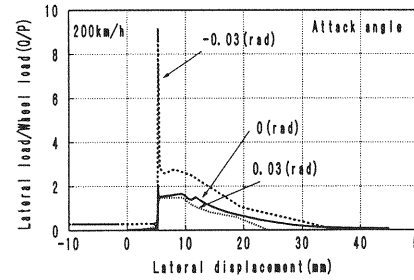

Fig.9 Q/P for lateral displacement of wheel

at it's acting points of axle spring as shown in **Fig.7**.

In case of $\psi_w=0$ with these forces, response curves for the Q/P at the rail contact point are shown in **Fig.8** where $\alpha=(t-t_0)/t_1$ with an idle time t_0 and a transient time t_1 being set here as 4 sec. and $F_v=F_h=60\text{kN}$.

The displacement of right-wheel illustrates repeatedly an 1 point contact state and a 2 point contact state between 1.5 and 3.7 sec., as shown in this figure with horizontal line. And the displacement of wheel increases rapidly, and it's vertical one reaches to the flange height 30mm after 4 sec.. At the same time, the Q/P gradually increases from 1 to 4.5 sec., then it is recognized that the mounting derailment occurs when it exceeds 2.0.

It is shown that a wheel flange mounting on the rail starts at the various amount of Q/P according to the different attack angles, and it continues even if Q/P may decrease when the mounting once started.

On the other hand, for the following forces in relation to the yaw angle of wheelset or so called attack angle, that is

$$F_v=F_h=60\text{kN} \quad \text{for } \psi_w\geqq 0,$$
$$F_v=120\text{kN},\quad F_h=240\text{kN} \quad \text{for } \psi_w<0,$$

displacements of wheel were calculated. Here, these forces are estimated so as to the mounting derailment appears to be sufficiently clear. In cases of $\psi_w=-0.03$, 0.0, 0.03 (rad), the Q/P in relation to the lateral displacement of wheel are shown in **Fig.9** where the running speed is 200km/h.

Maximum Q/P for the attack angle (-0.05 to 0.05 rad.) are shown in **Fig.10**, where the coefficient of friction μ are given 0.1 and 0.25. It is shown that the mounting limits in Q/P are 2.0 in

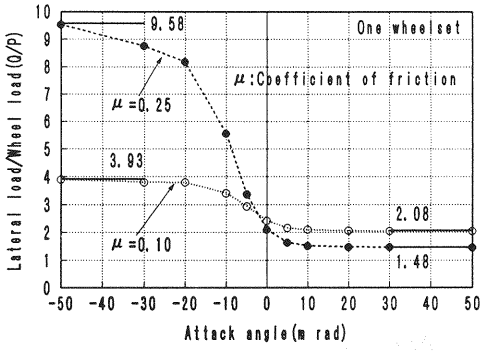

Fig.10 Mounting limit in Q/P for attack angle

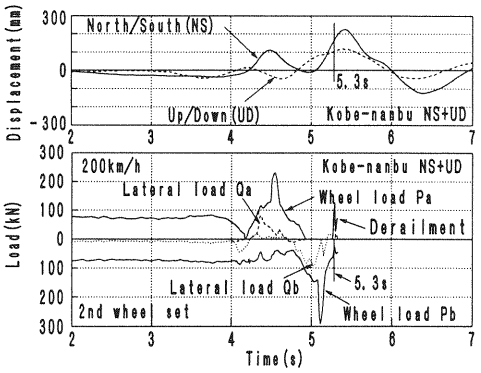

Fig.12 Response for Hyogo-Nanbu earth quake

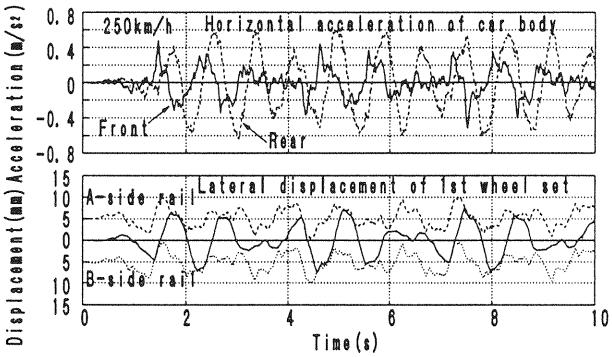

Fig.11 Response of vehicle on track irregularity

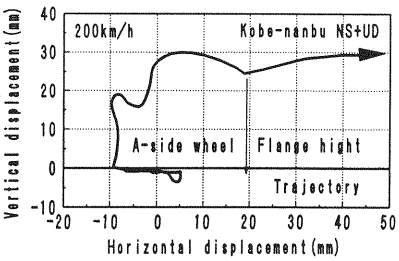

Fig.13 Wheelset movement (Hyogo-Nanbu earthquake)

case of $\psi_w = 0$,1.5 to 2 of positive attack angle but 4 to 9 of negative one. The derailment limit approaches the Nadal's value [9] as the absolute ψ_w increases.

(2) Simulation for track irregularities

A simulation will be shown for some track irregularities. The lateral displacement of the first wheelset and the lateral vibrational acceleration of the car body at the center of the first truck when the train is running at the speed of 250km/h are shown in **Fig.11** where the sample waves of irregular track using here were drawn from the power spectrum densities,

$$S(f_R) = 10^{-9} / f_R{}^3 (m^3) \quad \text{for lateral,}$$
$$S(f_R) = 2 \times 10^{-9} / f_R{}^3 (m^3) \quad \text{for vertical,}$$

where f_R denotes the space frequency.

As shown in this figure, the wheelset runs with lateral motion touching repeatedly the rail inside face. The lateral motion of the wheelset is nearly equal to the track in period, but its amplitude is larger than that of track. The lateral vibrational acceleration of car body is resemble to the lateral displacement of the wheelset in wave form, but it has sharp peaks at the wheel touching points to the rail.

(3) Simulation for the real earthquake

Response curves of the rear wheelset in the front truck (2nd wheelset) for the lateral and vertical motion of track transcribed from the NS (north/south) and UD (up/down) data of Hyogo-Nanbu earthquake(1.17,1995) are shown in **Fig.12**. The earthquake data was observed at the Kobe Observatory of the Meteorological Agency Japan where the vehicle speed is 200km/h.

The right-wheel once separates vertically from the rail after taking a peak in its wheel load at the beginning of the main earth quake motion. It moves rapidly outward the track, dropping on the rail top, and finally takes a large displacement to the rail at 5.3 sec., as shown in **Fig.13**.

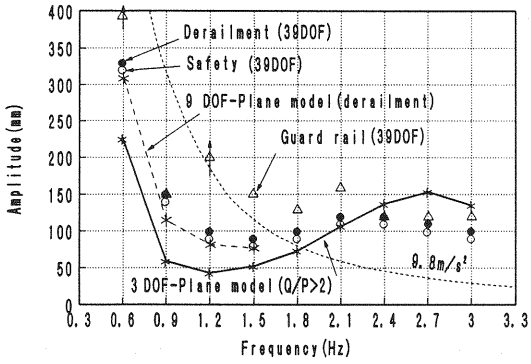

Fig.14 Derailment limit for track lateral vibration

These results almost coincide the last simulation results using the same parameters and same analytical assumptions except for the wheel/rail contact conditions [12].

(4) Tentative safety limit for the laterally oscillating track

The safety limit in amplitude of lateral vibration of track for given frequencies against derailment are computed by the new numerical method derived in this paper. And it is compared with other simpler methods as illustrated in **Fig.14** where the given lateral vibration to the track is an artificial wave that has a sinusoidal fundamental wave with 5 periods being multiplied by a half-sine function having a period of 10 times of the fundamental one.

The other methods being shown here are the Matsui's plane model with 3 degree-of-freedom (3DOF) [1], and a plane model with 9DOF which is obtained tentatively modifying the Matsui's model by adding vertical motions of car body, of truck and of wheelset, roll motions of truck and of wheelset and a lateral motion of truck.

The 3DOF model is the most simple one where the wheelset moves together with the rail, and only the ratio of Q/P(<2) is applied to running safety estimation. On the other hand, in the 9DOF model having vertical flanges, it is assumed that the wheel contacts with the rail through nonlinear creep forces, the rail moves together with the track, and the longitudinal parameters of vehicle are entirely neglected. And also the estimation of running safety is able to perform by the degree of wheel/rail separation as well as Q/P.

Computed results obtained by the simulation using the new model (39DOF model) are marked ○ for the safety and ● for the derailment in this diagram. As far as the derailment limit, the 39DOF model almost corresponds to the 9DOF model in case of lower frequency less than 1.5Hz. And also the 39DOF model gives a larger derailment limit than the 3DOF model. The simulation of 39DOF model gives a jumping derailment at the frequency lower than 1.2 Hz, a mounting derailment at the frequency higher than 1.5 Hz.

On the other hand, a trial simulation for estimating the mechanical effect of anti-derailment guard is performed where the gap between the back face of wheel flange and the anti-derailment guard is assumed to be $u_G = 0.03$m which is smaller than the standard gap, the spring constant of guard and its damping factor

$k_G = 15{,}000$kN/m , $c_G = 7.756$kNs/m ,

respectively.

As shown in the diagram, it will be said that the efficiency of the anti-derailment guard is recognized in the frequency range of 1.2 to 2.1Hz, but it is not recognized in the other frequency range.

7. CONCLUDING REMARKS

In relation to the safety estimation of vehicle running on a oscillating track, a new computing method which is able to pursue the movement up to the jumping or mounting derailment was proposed. The application of Kalker's theory and newly introduced 2 point contact algorithm at the wheel/rail contact point mainly enabled the direct derailment analysis.

A simulation result with this method up to the mechanical derailment was shown using real earthquake data. Further, it was shown that the jumping derailment occurs at the frequency lower than 1.2 Hz, but the mounting derailment occurs at higher than 1.5 Hz according to the simulation with the lateral vibration of track of which amplitude modified.

According to this analysis, in comparison with the results of *indirect* estimation of derailment previously obtained, the derailment limit of running vehicle on oscillating track shows large value as a whole. In case of 1.5Hz track lateral vibration,

amplitude of derailment limit of 55mm increases about till 80mm. This indicates an important meaning in practice.

Comparisons with simpler models were illustrated and efficiency of the anti-derailment guard was estimated tentatively. More precise estimation of parameters of vehicle models, spring constant or damper coefficient, stopper gap for example, remains as one of the future problems.

But it is still necessary to investigate the method how to increase the limit of running safety for the oscillating track caused by an earthquake having frequency about 1 Hz for jumping derailment. One of the effective methods for that will be a direct preventing by means of the anti-derailment guard. The determination of the practical structural details, however, remains unsolved. Further, it will be considered to investigate the effect of improvement of the vehicle dynamic property. It will be worthwhile to propose a more accurate dynamic model for anti-derailment guard and also the most appropriate simple model of vehicle for investigations on oscillating track for practical purpose.

ACKNOWLEGEMENT: A part of this paper is subsidized by the Ministry of Education, Science and Culture as 'the Foundation of Science Research 1997'.

REFERENCES

1) Matsuura,A., Tomita,K. and Wakui,H.: *Running safety of railway vehicle on oscillating track using a mechanical model with vertical wheel flanges*, (in Japanese) Trans. of J.S.C.E., No.556/I-38, pp.169-178, 1997.1.
2) Nishioka,T.: *A Theoretical Study on the Behavior of Railway Vehicle Considering Vibration of Tracks*, (in Japanese) Trans. of J.S.C.E., No.172, pp.43-57, 1969.12.
3) Nishioka,T. and Hashimoto,S.: *Running Stability of Two-axle Freight car on Bridges at Lateral Earthquake Shock*, (in Japanese) Trans. of J.S.C.E., No.296, pp.61-72, 1980.4.
4) Yasoshima,Y., Matsumoto,Y., Nishioka,T. and Oshima,K.: *Experimental Study of Running Stability of Railway Freight Cars on Vibrating Tracks*, (in Japanese) Trans. of J.S.C.E., No.313, pp.111-124, 1981.9.
5) Kalker,J.J.: *A Fast Algorithm for the Simplified Theory of Rolling Contact*, Vehicle System Dynamics, pp.1-13, 1982.11.
6) Yokose,K., Fukumoto,M. and Sado,T.: *Fundamental Consideration of Geometrical Contact between Wheel and Rail*, (in Japanese) Trans. of J.S.M.E.(C) Vol.56, No.528, pp.136-143, 1990.8.
7) Toyoda,M.: *Study on structure and performance of rail fastening device*, Railway Technical Research Report, No.861, Railway Technical Research Institute, (in Japanese) JNR, pp.27-30, 1973.8.
8) Hoshino,Y.: *A Practical Solution for Torsion of Rail*, (in Japanese) Trans. of J.S.C.E., No.210, pp.33-46, 1973.2.
9) Matsui,N., Koyama,M. and Nakamura,H.: *Running safety*,(in Japanese) Railway Technical Research Institute, JNR, -Study on High speed railways-, pp.253-267, 1967.3.
10) Timoshenko,S.: *Theory of Elasticity*, McGRAW -HILL, 1934.
11) Kalker,J.J.: *Survey of Wheel-rail Contact Theory*, Vehicle System Dynamics, pp.317-358, 1979.5.
12) Matsuura,A.: *Running safety of railway vehicle on oscillating track*, (in Japanese) Trans. of J.S.C.E for Hanshin-Awaji earthquake, pp.717-722, 1996.1.

(Received February 26,1997)